Case Studies in Thermal Engineering 41 (2023) 102665

Contents lists available at ScienceDirect

Case Studies in Thermal Engineering

journal homepage: www.elsevier.com/locate/csite

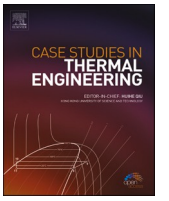

Experimental adjustment of the turbulent Schmidt number to model the evaporation rate of swimming pools in CFD programmes

Juan Luis Foncubierta Blázquez [a,*], Ismael R. Maestre [a], Francisco Javier González Gallero [a], L. Pérez-Lombard [b], Michele Bottarelli [c]

[a] Escuela Técnica Superior de Ingeniería de Algeciras, Universidad de Cádiz, Avenida Ramón Puyol, s/n, Algeciras, 11202, Spain
[b] Grupo de Termotecnia, Escuela Superior de Ingenieros, Universidad de Sevilla, Camino de los Descubrimientos, 41092, Sevilla, Spain
[c] Department of Architecture, University of Ferrara, Via Quartieri 8, Ferrara, 44121, Italy

ARTICLE INFO

Handling Editor: Y Su

ABSTRACT

Water evaporation rate is among the most significant parameters to design and select air conditioning systems in buildings with indoor swimming pools. Experimental correlations are today widely used to estimate water evaporation rate, although discrepancies of up to 80% among existing correlations have been shown. An alternative to these empirical methods is the calculation of evaporation rate through computer fluid dynamics techniques. One of the most significant parameters to solve the mass transfer at the air-water interface in these models is the value of the turbulent Schmidt number. Although this value depends on air and water conditions (i.e., temperatures, velocities, and vapour pressure, among others), commercial computer fluid dynamics programmes set a fixed value by default. This study presents a new value through an experimental adjustment. A total of 40 experimental tests have been performed in a wind tunnel under typical conditions in indoor swimming pools. Afterwards, the adjustment was validated with data from 145 experimental tests reported in the scientific literature. The mean relative error in the evaporation rate using the turbulent Schmidt number was 7%, as against 25% using the value by default. The maximum error was reduced from 35% to 15% in forced convection regime.

Nomenclature

α	Thermal diffusivity [m^2/s]	D	Thermal diffusivity [m^2/s]
D	Mass diffusivity [m^2/s]		
E	Evaporation rate [$kg/(s \cdot m^2)$]		
Gr	Grashof number [−]		
ν	Kinematic viscosity [m^2/s]	*Pe*	Kinematic viscosity [m^2/s]
Pe	Peclet number [−]		
Pr	Prandtl number [−]		
Re	Reynolds number [−]		
RH	Relative humidity [%]		
Sc	Schmidt number [−]		

* Corresponding author.
E-mail address: juanluis.foncubierta@uca.es (J.L. Foncubierta Blázquez).

https://doi.org/10.1016/j.csite.2022.102665
Received 9 November 2022; Received in revised form 15 December 2022; Accepted 21 December 2022
Available online 22 December 2022

T	Temperature [C]
τ	Shear stress [N/m^2]
u	Velocity [m/s]
V	Velocity [m/s]

Subscripts

a	Air
exp	Experimental
t	Turbulent
I	Interface
sim	Simulated
w	Water

Acronyms

CFD	Computational Fluid Dynamics
RANS	Reynolds Averaged Navier Stokes equations

1. Introduction

The use of air conditioning systems in indoor swimming pools to maintain comfort conditions in both water and air could represent 60% of the total consumption of thermal installations in buildings [1]. These systems should replenish the heat loss in the water of the basin, mainly latent in nature due to water evaporation, as well as remove the excess of air humidity originated by that evaporation. Accordingly, the evaporation rate (E) of swimming pools is among the main parameters to consider when selecting and designing these systems, and it is expressed in terms of water mass flow per surface unit (kg/s·m^2).

The evaporation phenomenon is a local complex mechanism, and its analysis requires knowing the pressure and velocity within temperature, vapour concentration and velocity boundary layers along water surface. Similar heat and mass transfer phenomena were successfully resolved in fields such as nanofluids applications [2], non-Newtonian fluids [3], water flows around skin models [4] and airflows around fins [5]. Specifically, evaporation phenomenon is developed by the diffusive component described by the Fick's law considering concentration and partial pressure gradients in the boundary layer and by the advective component induced by velocity gradients [6].

There are theoretical methods based on both the transitional probability concept [7] or the kinetic theory of gases [8] to calculate E. However, empirical methods based on correlations have been developed as thermodynamic variables within the boundary layer are uncertain. Unlike theoretical methods, experimental correlations associate the evaporation rate with the properties of the bulk air flow such as velocity, temperature and relative humidity, as well as with mean water temperature ([9–14]).

In an indoor swimming pool, there are regions, such as those close to ventilation systems, where forced convection predominates, as well as regions where airflow is driven by natural convection, such as the air in contact with the water surface. As Shah [12] stated, most published correlations only consider forced convection conditions. On the other hand, the heterogeneity of experimental methodologies and the lack of a rigorous dimensional analysis (see reviews [15,16]) result in discrepancies between correlations of up to 80% under the same air and water conditions [17]. Nevertheless, experimental correlations are the most used methodology to estimate E.

Some authors have proposed the use of numerical methods based on computer fluid dynamics (CFD) techniques as these methods model airflow distribution in turbulent regime (including the boundary layer in the interface), coupled to air conditioning systems. In general, these methods numerically solve the equations of both species transport and the linear momentum and energy on a control volume made up of the air that is usually modelled as the mixture of two gases, i.e., dry air and water vapour, with the modelling of the boundary condition in the swimming pool air-water interface being crucial.

Likewise, an imposed vapour flow estimated by experimental correlations have been used as boundary condition in the air-water interface ([17–19]). Temperature distribution and air humidity can be calculated, but these models do not provide an additional advantage to estimate E vis-à-vis correlations. Ciuman et al. [20] experimentally validated a CFD model to determine temperature, humidity, and airflow velocity conditions in an actual swimming pool. Various experimental correlations were tested as boundary condition in the air-water interface. In this case, the VDI correlation [21] predicted the measured air profile satisfactorily, while other correlations obtained errors of up to 48%.

To not depend on experimental correlations, other CFD methodologies have also been developed to estimate evaporation rate. Limane et al. [22] developed a three-dimensional model of an actual swimming pool to predict air velocity, humidity, and temperature profiles. The interface was modelled considering the thermal equilibrium between air and water and imposing saturation conditions on the air of the interface. A similar boundary condition was used by Min et al. [23] to predict airflow conditions. Hence, E is not considered a constant and uniform value but the result of interactions in the interface according to local flow conditions, which are generally turbulent. Turbulence increases transport properties (i.e., kinematic viscosity, thermal diffusivity, and mass diffusivity, among others) [24], so the estimated E could be sensitive to the parameters that configure the turbulence models used in CFD.

In this regard, the most used turbulent models are based on the time-averaged equations of motion for fluid flow, i.e., Reynolds

averaged Navier Stokes equations (RANS) [25], in which k-ε [26], k-ω [27] and derivative models [28] could be stressed. These models assume the gradient diffusion hypothesis to estimate the Reynolds stress tensor according to equation (1):

$$-\overline{u_i' u_j'} = \nu_t \frac{\partial \overline{u_i}}{\partial x_j} \tag{1}$$

Where ν_t is turbulent kinematic viscosity, understood as the increase in viscosity due to turbulence. An effective viscosity could therefore be defined as the sum of the molecular viscosity and the turbulent viscosity. The other transport properties are often expressed as a function of ν_t as in equations (2) and (3):

$$\alpha_t = \frac{\nu_t}{Pr_t} \tag{2}$$

$$D_t = \frac{\nu_t}{Sc_t} \tag{3}$$

Where α_t, D_t, Pr_t, and Sc_t are thermal diffusivity, mass diffusivity, the turbulent Prandtl number and the turbulent Schmidt number, respectively.

RANS turbulent models calculate the turbulent viscosity according to flow conditions (i.e., flow physics properties, turbulent kinetic energy and dissipation, among others), and the values of thermal and mass diffusivity are defined by the turbulent Prandtl and Schmidt numbers (Eqs. (2) and (3)) which are considered as constant values. Both Pr_t and Sc_t have been adjusted through experimental tests. The most significant experimental tests related to Sc_t are included below due to the strong dependence of E on this parameter.

One of the most important studies is that by Spalding et al. [29], which tested the concentration distribution of a gas in a round turbulent free jet discharged in a reservoir with another gas with the same density. The Sc_t of the turbulent CFD model was adjusted by measuring the dispersion of the gas included in the receptor gas, thus reducing the error between numerical and experimental results. Finally, a value of Sc_t of 0.7 was established as it is widely used as the value by default in most commercial CFD software [30].

However, different values of Sc_t were later obtained. Colli et al. [31] adjusted this value by using the SST (shear-stress transport) turbulent model [28] to model the mass transfer in a electrochemical reactor under laminar and turbulent flow conditions in rectangular and tubular ducts, obtaining a value of Sc_t of 0.5. Launder et al. [26] stated that the value of Sc_t could vary near walls, so a value of 0.9 was proposed for these cases. Galeev et al. [32] predicted the evaporation of high volatile fluids through both a CFD RANS model and an optimised Sc_t of 0.7. However, these authors previously proposed values of 0.5 for neutral gases, recommending 0.7 for heavy gases [33]. Likewise, Tominaga et al. [34] reviewed many experimental studies focused on adjusting Sc_t. These studies were divided into various applications: jets, turbidity currents, plume dispersion in boundary layer, and dispersion around buildings. The high dispersion degree of the values, from 0.2 to 0.9, induces us to conclude that the optimum Sc_t should not be standard as it depends on the application and flow conditions.

This study focuses on evaporation in swimming pools, so the CFD model implemented by Raimundo et al. [35] should be stressed. This model was based on the k-ε turbulent model in which the evaporation rate was estimated by a concentration wall-function developed considering the analogy with that used to solve the velocity profile in the boundary layer. The model was validated by the experimental data obtained in a wind tunnel of a square cross-section of 0.4 m × 0.4 m and 3.3 m long, obtaining a mean error of around 7%. To adjust the value of Sc_t, the expression by Myong et al. [36] was unsuccessfully used (function of Sc and molecular Pr), mainly because most experimental tests were out of the limit or in the range limit to apply the expression (10^4<Re < 10^5). Moreover, this expression did not consider local flow conditions. Accordingly, Raimundo et al. proposed another correlation that related the Sc_t to the module of the flow velocity.

Foncubierta et al. [37] developed a CFD model based on three hypotheses applied to the air-water interface: thermal equilibrium, completely saturated air in the interface, and concentration boundary layer greater than the velocity boundary layer. The SST turbulent model and a constant Sc_t of 0.7 were used, so the model obtained errors lower than 10% for natural and mixed convection regimes ($1.5 < Gr/\mathrm{Re}^2 < 5$). However, the error was up to 45% for forced convection regimes ($Gr/\mathrm{Re}^2 < 1.5$).

This study improves the methodology proposed by Foncubierta et al. [37] by adjusting Sc_t through experimental data and under typical air and water conditions in indoor swimming pools. Firstly, the corrected method is described. Secondly, Sc_t is adjusted using the experimental data obtained in a wind tunnel. Finally, the results are validated with the experimental data from Jodat et al. [14,38] and Raimundo et al. [35].

2. Methodology

The stages taken to adjust Sc_t were as follows: 1) definition of the base model (Foncubierta et al. [37]) from which Sc_t was adjusted; 2) experimental development required to adjust the model within the range of $Gr/\mathrm{Re}^2 < 1.5$, particularly from 0.007 to 0.075; 3) numerical modelling of the experimental test; 4) adjustment of Sc_t, and 5) model validation by using experimental tests from the scientific literature.

Since convection regime plays an important role in both heat and mass transfer [6], the results obtained here will be shown in terms of the ratio Gr/Re^2, which compares natural and forced convection strengths. Thus, flows with $Gr/\mathrm{Re}^2 < 0.1$ could be considered forced convective flows; mixed convection flow regime for $0.1 < Gr/\mathrm{Re}^2 < 5$; and free convection for $Gr/\mathrm{Re}^2 > 5$ [14].

2.1. Brief description of the base model

The major hypothesis on which the model was based was that, under typical velocity and air temperature conditions in indoor swimming pools, there could be a thin stable layer of saturated air over the water surface and in thermal equilibrium with it. Thus, the vapour flow from this layer to the surrounding air through diffusion and advection mechanisms would be the same as that from the evaporation mechanism in the air-water interface. Water domain was therefore not modelled because the conditions between the interface of the saturated layer and the remaining air were steady and known. Moreover, control volume was defined by the room air of the swimming pool until the interface of the saturated layer in which boundary conditions were established as follows: 1) temperature imposed and equal to the water temperature of the swimming pool; 2) saturation, relative humidity 100%; and 3) free slip condition ($\tau = 0$) (see Table 1). The third aspect could be justified because the Schmidt number is often lower than 1 in this type of flow conditions (stable layer with low velocity), thus implying that the thickness of the concentration boundary layer is lower than the velocity boundary layer. The equations of continuity (4), linear momentum (5) and energy (6) that govern the problem are the following:

$$\frac{\partial}{\partial t}(\rho Y) + \vec{\nabla} \cdot (\rho Y \vec{v}) = -\vec{\nabla} \cdot \vec{j} \tag{4}$$

$$\vec{\nabla} \cdot (\rho \vec{v} \vec{v}) = -\vec{\nabla} P + \vec{\nabla} \cdot \vec{\tau} + \rho \vec{g} \tag{5}$$

$$\vec{\nabla} \cdot (\rho h \vec{v}) = -\vec{\nabla} \cdot \vec{q} + \vec{v} \cdot \vec{\nabla} P + \vec{\tau} : \nabla \vec{v} + S_h \tag{6}$$

Where:

$$S_h = \vec{\nabla} \cdot \left(\sum h_i \vec{j}_i \right) \tag{7}$$

$$\rho = \sum Y_i \rho_i \tag{8}$$

$$h = \sum Y_i h_i \tag{9}$$

Further information can be found in Refs. [15,37]. Equations (7)–(9) stands for the ideal gas homogeneous mixture model. Mixture density (8) and enthalpy (9) are calculated as mass fraction averages.

The numerical solution of the model through CFD techniques was proposed, and the air was modelled as a mixture of two ideal gases (dry air and water vapour). The species transport and velocity and temperature profiles were solved by using the multicomponent model [30]. The SST turbulent model was used by applying a mesh refinement to the air-water interface until reaching a value of y + lower than 1. The absolute residual of mass conservation equations should be at least of two magnitude commands lower than the calculated evaporation rate, which could be estimated by the equilibrium of the water mass in the domain.

The value of Sc_t in the base model was fixed to 0.7. The next section describes the methodology to adjust this parameter, which is the goal of this study.

2.2. Experimental procedure

The experimental test consisted of a square section wind tunnel 30 cm wide and 100 cm long (Fig. 1). Air velocity was adjusted with a variable speed drive placed in the fan at the beginning of the tunnel. Air conditions were regulated by both an evaporator of a simple compression cycle regulated by a PID control on the impulsion temperature and electrical resistances regulated in the same way. A filter was placed at 40 cm from the fan outlet to homogenise the airflow from the batteries. An aluminium pan of 32.5 cm × 23.5 cm × 3.5 cm containing the water to evaporate was placed at the outlet of the tunnel. Water temperature was regulated by an electrical resistance of 200W placed under the pan with an on/off control. Temperature and relative humidity sensors were model Testo 174H, with a measurement accuracy of ±0.5 °C and ±3%, respectively. The water temperature probe was an NTC sensor, with an accuracy of 0.1 °C. Air velocity was measured by a Testo 435-4 hot-wire probe, with a measurement uncertainty of ±0.03 m/s plus 4% of the measured value. After reaching steady conditions, the pan with water was weighed on scales with an accuracy degree of ±1 g. One hour after starting the experiment, the pan was put apart, and the evaporated water was calculated from the difference of the final and initial weight. According to these data, the mean global error was 4.1%. Further information can be found in Ref. [15].

A total of 40 experimental tests were performed with air temperature ranges from 28% to 68 °C, water temperature 2 °C below air temperature, relative humidity from 50% to 70%, and air intake velocities from 0.55 m/s to 1.02 m/s. The ratio Gr/Re_L^2 was always lower than 0.08. Table 2 shows the results obtained in the evaporation rate (E_{exp}).

Table 1
Boundary conditions at the air-water interface for the base and enhanced models.

	Base model	Enhanced Model
Conditions at the air-water interface	- $T_I = T_w$ - $Y_I = Y_w$ - $\tau_I = 0$ (*free slip wall*) - $Sc_t = 0.7$	- $T_I = T_w$ - $Y_I = Y_w$ - $\tau_I = 0$ (*free slip wall*) - Sc_t = New adjusted value

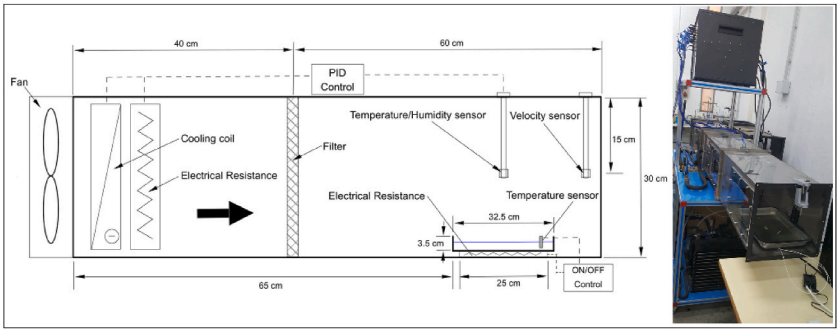

Fig. 1. Experimental scheme.

Table 2
Experimental conditions and evaporation rates.

Nº	V_a (m/s)	T_a (°C)	T_w (°C)	RH (%)	E_{exp} (kg/m^{2}h)	Gr/Re_L^2
1	0.55	26.1	23.9	47.3	0.236	0.036
2		26.0	23.9	58.3	0.170	0.037
3		27.1	25.0	54.0	0.223	0.042
4		26.9	25.1	57.7	0.209	0.053
5		28.0	26.0	55.1	0.236	0.052
6		28.2	25.9	55.4	0.223	0.044
7		29.1	27.2	53.1	0.262	0.064
8		29.2	27.0	53.2	0.419	0.052
9		30.1	28.1	48.3	0.314	0.067
10		30.0	28.2	49.6	0.314	0.075
11	0.7	26.2	24.1	44.2	0.327	0.023
12		26.3	24.1	57.7	0.223	0.021
13		26.9	25.1	58.0	0.262	0.032
14		27.4	25.1	57.3	0.236	0.024
15		28.2	26.1	55.3	0.275	0.030
16		28.4	26.0	53.6	0.288	0.026
17		29.1	27.1	49.2	0.354	0.037
18		29.1	27.2	45.7	0.393	0.039
19		30.0	28.0	39.6	0.458	0.041
20		30.1	27.9	36.2	0.458	0.037
21	0.85	26.2	24.1	68.1	0.471	0.015
22		26.0	24.1	68.5	0.183	0.018
23		27.0	25.1	65.0	0.223	0.021
24		27.0	25.3	61.1	0.275	0.023
25		28.0	26.2	58.5	0.301	0.024
26		28.1	26.2	58.4	0.563	0.024
27		29.0	27.4	55.2	0.354	0.031
28		28.8	27.0	52.6	0.393	0.028
29		30.1	28.1	50.1	0.432	0.029
30		30.1	28.2	50.6	0.406	0.030
31	1.02	26.2	24.2	52.2	0.367	0.012
32		26.4	23.9	52.9	0.327	0.007
33		27.0	24.8	52.2	0.550	0.011
34		27.2	25.1	51.9	0.380	0.012
35		28.0	25.9	54.6	0.615	0.015
36		28.1	26.3	53.9	0.406	0.018
37		29.1	27.1	48.2	0.668	0.018
38		29.2	27.2	50.7	0.458	0.018
39		30.1	28.0	38.8	0.720	0.019
40		30.0	28.0	28.3	0.707	0.020

2.3. Numerical modelling

The numerical modelling is similar to that used by Foncubierta et al. [37]: a two-dimensional CFD modelling of a longitudinal section of the tunnel carried out using Ansys Fluent 18. The inlet was modelled with the velocity imposed and equal to that measured in the experimental test, the outlet was modelled with constant atmospheric pressure, and walls were imposed with both the no-slip condition and zero gradient in the normal direction. The conditions described in Section 2.1. were applied at the air-water interface. The resolution algorithm was SIMPLE (Semi-Implicit Method for Pressure Linked Equations) with second order upwind numerical

scheme. Likewise, the SST turbulent model was used. The resolution process continued until the error in mass conservation was at least two magnitude commands lower than the calculated evaporation rate.

A grid independence study was carried out refining the mesh until meeting two criteria: 1) the variation of the evaporation rate compared to the previous mesh was lower than 5%; and 2) the y+ in the surface of water was close to 1.

2.4. Turbulent Schmidt number adjustment

The experimental tests included in Table 2 were numerically modelled with 10 values of Sc_t, from 0.1 to 1. Fig. 2 shows the error evolution in the numerical evaporation rate compared to the experimental one in two representative cases (0.55 m/s and 1.02 m/s). There was a minimum error for a Sc_t of 0.2, where the error was around 1%. This situation was repeated in the remaining experimental tests. A constant Sc_t of 0.2 was therefore set in the model as result of the adjustment.

Fig. 3 shows the evaporation rate obtained through the numerical simulation in contrast to the experimental evaporation rate (Table 2) of the base and enhanced models. The results obtained by the enhanced model were adjusted to the experimental data with an error lower than 10%, as against the maximum error of 34% for the base.

There was no trend of the error evolution as a function of the ratio Gr/Re_L^2 (Fig. 4). The mean relative error in the enhanced model was 6.75%, with a standard deviation of 2.3%, as against 29% and 4.76%, respectively, in the base model.

2.5. Model validation

The model was validated by using the experimental data from Raimundo et al. [35] and Jodat et al. [14]. Raimundo et al. [35] performed 28 experimental tests in a wind tunnel of 3.3 m length, with an evaporation surface of 0.15 m^2, under indoor pools typical conditions. Air velocities were from 0.1 m/s to 0.7 m/s, and Gr/Re_L^2 was from 0.2 to 42. In order to carry out a robust validation, the enhanced model was tested using those experiments from Jodat et al. [14] for which the base model obtained the worst results. Thus, 117 experimental tests performed in a tunnel with a total length of 1.5 m and a velocity range from 4 m/s to 6 m/s were used. The ratio Gr/Re_L^2 varied from $9{\cdot}10^{-4}$ to 0.09 (Fig. 5).

Fig. 6 shows the simulated evaporation rate compared to the experimental rate for the base and enhanced models. The adjustment obtained in Section 3.1 (adjustment cases) was maintained when the model was applied to the other validation cases. The mean relative error was therefore around 7% for the enhanced model, whereas it was 25% for the base model. Fig. 7 analyses the relative error distribution as a function of the evaporation rate. From 2 $kg/m^2{\cdot}h$ onward, distribution was constant in ranges from 5% to 1% and from 32% to 20% for the enhanced and base models, respectively. In ranges lower than 2 $kg/m^2{\cdot}h$, the range was similar in both models, but the mean error was 10% for the enhanced model and 27% for the base model.

Fig. 8 represents the relative error distribution in terms of the ratio Gr/Re_L^2. The enhanced model presented a reduction of the relative error under forced convection conditions ($Gr/Re_L^2<0.1$). In these cases, the mean relative error of the enhanced model was 6%, as against 30% of the base model. Likewise, regimes with $Gr/Re_L^2>0.1$ did not show significant differences.

3. Conclusions

The evaporation rate in indoor swimming pools is usually calculated using experimental correlations, although discrepancies of up to 80% have been found among them. Another alternative for estimating the evaporation rate is numerical simulation based on CFD techniques, where the turbulent Schmidt number (Sc_t) is a relevant parameter in the modelling of mass transfer problems. From the studies reviewed in the scientific literature, it is clear that this value depends on the application and flow conditions under consideration.

In the present work, a value of Sc_t is proposed to estimate the evaporation rate in unoccupied indoor swimming pools. This value was adjusted through 40 experimental tests performed in a wind tunnel and under various velocity (from 0.55 m/s to 1.02 m/s), air temperature (from 26 °C to 30 °C), relative humidity (from 28% to 68%), and water temperature (from 24 °C to 28 °C) conditions in forced convection regime ($Gr/Re^2 < 0.1$). Furthermore, the enhanced model was validated through 145 additional experimental tests from the scientific literature with an extended range of flow regimes ($0.001 < Gr/Re^2 < 100$).

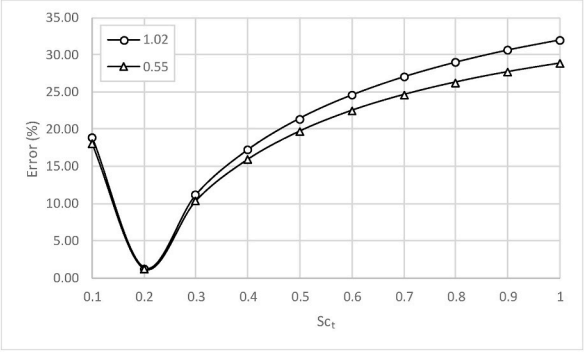

Fig. 2. Evaporation rate error as a function of Sc_t for velocities of 0.55 m/s and 1.02 m/s.

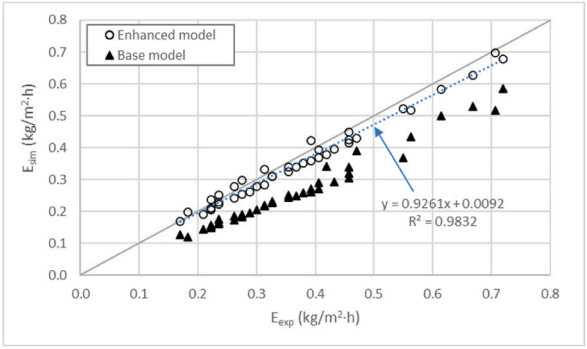

Fig. 3. Evaporation rate obtained by simulating adjustment cases as a function of the experimental rate for the base and enhanced models.

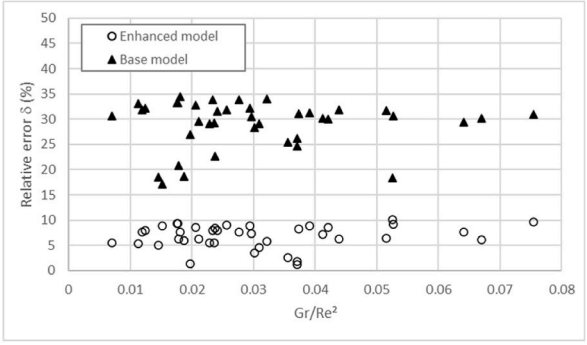

Fig. 4. Relative error of the adjustment cases as a function of the ratio Gr/Re_L^2 for the base and enhanced models.

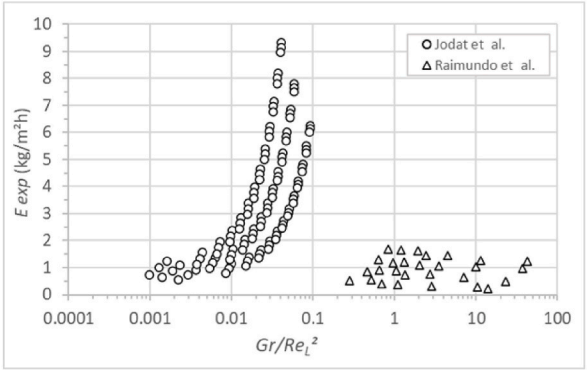

Fig. 5. Evaporation rate results as a function of Gr/Re^2 for Jodat et al. and Raimundo et al. experimental tests.

The main conclusions drawn from the present work are the following:

- The optimum value of Sc_t that minimises the difference between the estimated and experimental evaporation rate was 0.2 in all cases, thus obtaining a mean relative error of 6.9%.
- Likewise, the proposed turbulent Schmidt number of 0.2 significantly improved the turbulent Schmidt number set by default by commercial CFD programmes of 0.7, thus reducing the mean relative error from 25% to 7% in the validation cases.
- The maximum error was reduced from 35% to 15% in forced convection regime ($Gr/\mathrm{Re}^2 < 0.1$).

Finally, and despite the existing uncertainty concerning its correct specification, the authors would recommend setting the Sc_t to 0.2 in the estimation of the water evaporation rate in unoccupied indoor swimming pools through numerical CFD techniques within the range studied.

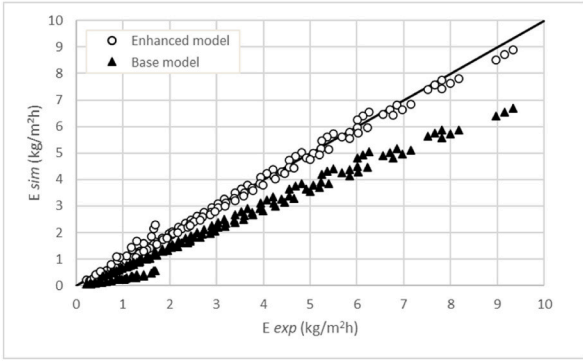

Fig. 6. Comparison of experimental and estimated values of the evaporation rates for validation cases (base and enhanced models).

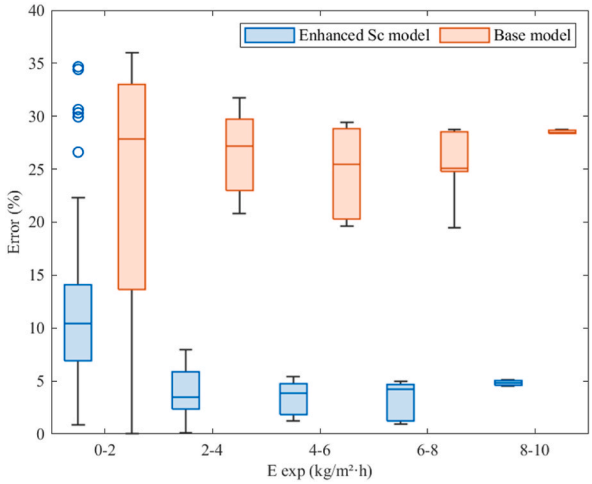

Fig. 7. Error distribution obtained by simulating validation cases as a function of the experimental rate for the base and enhanced models.

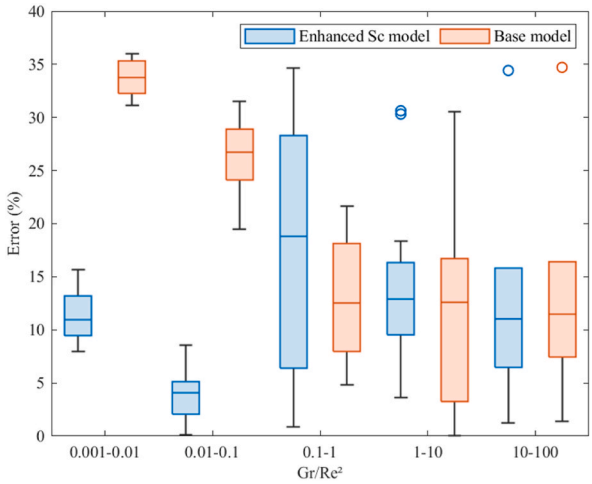

Fig. 8. Distribution of the error obtained by simulating validation cases as a function of Gr/Re_L^2 for the base and enhanced models.

Author statement

Juan Luis Foncubierta Blázquez: *Conceptualization, Investigation, Writing - Original Draft.* **Ismael R. Maestre**: *Conceptualization, Writing - Review & Editing, Supervision.* **Francisco Javier González Gallero**: *Methodology, Writing - Review & Editing.* **L. Pérez-**

Lombard: *Methodology, Writing - Review & Editing.* **Michele Bottarelli**: *Writing - Review & Editing.*

Declaration of competing interest

The authors declare that they have no known competing financial interests or personal relationships that could have appeared to influence the work reported in this paper.

Data availability

Data will be made available on request.

References

[1] Atecyr, DTIE 10.06 Piscinas Cubiertas. Sistemas de climatización, deshumectación y ahorro de energía mediante bombas de calor.
[2] A. Ullah, Ikramullah, M.M. Selim, T. Abdeljawad, M. Ayaz, N. Mlaiki, A. Ghafoor, A magnetite–water-based nanofluid three-dimensional thin film flow on an inclined rotating surface with non-linear thermal radiations and couple stress effects, Energies 14 (2021) 5531.
[3] S. Khan, M.M. Selim, A. Khan, A. Ullah, T. Abdeljawad, Ikramullah, M. Ayaz, W.K. Mashwani, On the analysis of the non-Newtonian fluid flow past a stretching/shrinking permeable surface with heat and mass transfer, Coatings 11 (2021) 566.
[4] M. Turkyilmazoglu, Heat transfer from warm water to a moving foot in a footbath, Appl. Therm. Eng. 98 (2016) 280–287.
[5] M. Turkyilmazoglu, Thermal management of parabolic pin fn subjected to a uniform oncoming airfow: optimum fn dimensions, J. Therm. Anal. Calorim. 143 (2021) 3731–3739, https://doi.org/10.1007/s10973-020-10382-x.
[6] F.P. Incropera, D.P. DeWitt, Fundamentals of Heat and Mass Transfer, J. Wiley, New York, 2002.
[7] C.A. Ward, G. Fang, Expression for predicting liquid evaporation flux: statistical rate theory approach, Phys. Rev. E 59 (1) (1999) 429–440.
[8] V. Badam, V. Kumar, F. Durst, K. Danov, Experimental and theoretical investigations on interfacial temperature jumps during evaporation, Exp. Therm. Fluid Sci. 32 (2007) 276–292.
[9] M. Shah, Evaluation of methods for prediction of evaporation from water pools, J. Build. Phys. (July 2021).
[10] C. Smith, R. Jones, G. Löf, Energy requirements and potential savings for heated indoor, Build. Eng. 99 (1993) 864–874.
[11] M. Pauken, An experimental investigation of combined turbulent free and forced evaporation, Exp. Therm. Fluid Sci. 18 (1999) 334–340.
[12] M. Shah, Methods for calculation of evaporation from swimming pools and OtherWater surfaces, Build. Eng. 120 (2) (2014).
[13] F. Asdrubali, A scale model to evaluate water evaporation from indoor swimming pools, Energy Build. 41 (2009) 311–319.
[14] A. Jodat, M. Moghiman, M. Anbarsooz, Experimental comparison of the ability of Dalton based and similarity theory correlations to predict water evaporation rate in different convection regimes, Heat Mass Tran. 48 (2012) 1397–1406.
[15] J.L. Foncubierta Blázquez, I.R. Maestre, F.J. González Gallero, P. Álvarez Gómez, Experimental test for the estimation of the evaporation rate in indoor swimming pools: validation of a new CFD-based simulation methodology, Build. Environ. 138 (2018) 293–299.
[16] M. Shah, Analytical formulas for calculating water evaporation from pools, Build. Eng. 114 (2) (2008).
[17] Z. Li, P. Heiselberg, CFD Simulations for Water Evaporation and Airflow Movement in Swimming Baths Indoor Environmental Engineering, Report for the Project Optimization of Ventilation System in Swimming Bath, 2005. Denmark.
[18] M. Liu, K. Wittchen, P. Heiselberg, Control strategies for intelligent glazedfac, ade and their influence on energy and comfort performance of officebuildings in Denmark, Appl. Energy (2015) 43–51.
[19] P. Koper, B. Lipska, W. Michnol, Assessment of thermal comfort in an indoor swimming-pool, Architect. Civil Eng. Environ. 3, 95-104 (2010).
[20] P. Ciuman, B. Lipska, Experimental validation of the numerical model of air, heat and moisture flow in an indoor swimming pool, Build. Environ. 145 (2018) 1–14.
[21] VDI, Wärme, Raumlufttechnik, Wasserer- und –entsor-gung in Hallen und Freibädern, VDI, 2022.
[22] A. Limane, H. Fellouah, N. Galanis, Simulation of airflow with heat and mass transfer in an indoor swimming pool by OpenFoam, Int. J. Heat Mass Tran. 109 (2017) 862–878.
[23] J. Min, Y. Tang, Theoretical analysis of water film evaporation characteristics on an adiabatic solid wall, Int. J. Refrig. 53 (2015) 55–61.
[24] B.E. Launder, Heat and mass transport, in: P. Bradshaw (Ed.), Turbulence. Topics in Applied Physics, vol. 12, Springer, Berlin, 1976. https://doi.org/10.1007/978-3-662-22568-4_6.
[25] O. Reynolds, On the Dynamical Theory of Incompressible Viscous Fluids and the Determination of the Criterion, vol. 186, Philosophical Transactions of the Royal Society of London A., 1895, pp. 123–164.
[26] B. Launder, D. Spalding, The numerical computation of turbulent flows, Comput. Methods Appl. Mech. Eng. 3 (2) (1974) 269–289.
[27] D.C. Wilcox, Turbulence Modeling for CFD, second ed., DCW Industries, 1998.
[28] F.R. Menter, Two-equation eddy-viscosity turbulence models for engineering applications, AIAA J. 32 (8) (1994) 1598–1605.
[29] D. Spalding, Concentration fluctuations in a round turbulent free jet, J. Chem. Eng. Sci. 26 (1971) 95–107.
[30] Ansys® Fluent, Release 18, Help System, Theory Guide, ANSYS, Inc.".
[31] A.N. Colli, J.M. Bisang, A CFD study with analytical and experimental validation of laminar and turbulent mass-transfer in electrochemical reactors, J. Electrochem. Soc. 165 (2) (2018) E81–E88.
[32] A. Galeev, A. Salin, S. Ponikarov, Numerical simulation of evaporation of volatile liquids, J. Loss Prev. Process. Ind. 38 (2015) 39–49.
[33] A. Galeev, A. Salin, S. Ponikarov, Consequence analysis of aqueous ammonia spill using computational fluid dynamics, J. Loss Prev. Process. Ind. 26 (4) (2013) 628–638.
[34] Y. Tominaga, T. Stathopoulos, Turbulent Schmidt numbers for CFD analysis with various types of flowfield, Atmos. Environ. 41 (37) (2007) 8091–8099.
[35] A.M. Raimundo, A.R. Gaspar, A.V.M. Oliveira, D.A. Quintela, Wind tunnel measurements and numerical simulations of water evaporation in forced convection airflow, Int. J. Therm. Sci. 86 (2014) 28–40.
[36] H.K. Myong, N. Kasagi, M. Hirata, Numerical prediction of turbulent pipe flow heat transfer for various Prandtl number fluids with the improved k-e turbulence model, JSME Int. J. 32 (4) (1989) 613–622.
[37] J.L. Foncubierta Blázquez, I.R. Maestre, F.J. González Gallero, P. Álvarez Gómez, A new practical CFD-based methodology to calculate the evaporation rate in indoor swimming pools, Energy Build. 149 (2017) 133–141.
[38] A. Jodat, M. Moghiman, An experimental assessment of the evaporation correlations for natural, forced and combined convection regimes, in: Proc. IMechE Vol. 226 Part C: J. Mechanical Engineering Science, 2011.